Role of γ-Carboxyglutamic Acid in the Calcium-Induced Structural Transition of Conantokin G, a Conotoxin from the Marine Snail *Conus geographus*[†,‡]

Alan C. Rigby,[§,||] James D. Baleja,[§] Leping Li,[⊥] Lee G. Pedersen,[⊥] Barbara C. Furie,[§,||,▽] and Bruce Furie*[,§,||,▽]

Marine Biological Laboratory, Woods Hole, Massachusetts 02543, Center for Hemostasis and Thrombosis Research, Division of Hematology−Oncology, New England Medical Center, and Departments of Medicine and Biochemistry, Tufts University School of Medicine, Boston, Massachusetts 02111, National Institute of Environmental Health Sciences, Research Triangle Park, North Carolina 27709, and Department of Chemistry, University of North Carolina, Chapel Hill, North Carolina 27599

Received July 30, 1997; Revised Manuscript Received October 7, 1997[⊗]

ABSTRACT: Conantokin G is a γ-carboxyglutamic acid- (Gla-) containing conotoxin isolated from the venom of the marine cone snail *Conus geographus*. This 17-residue polypeptide, which contains five γ-carboxyglutamic acid residues, is a *N*-methyl-D-aspartate- (NMDA-) type glutamate receptor antagonist. To investigate the role of γ-carboxyglutamic acid in the calcium-induced structural transition of conantokin G, we determined the three-dimensional structure of the conantokin G/Ca^{2+} complex by two-dimensional ^{1}H NMR spectroscopy and compared it to the high-resolution structure of conantokin G in the absence of metal ions [Rigby et al. (1997) *Biochemistry 36,* 6906]. Complete resonance assignments were made by two dimensional ^{1}H NMR spectroscopy at pH 5.6 in the presence of saturating amounts of Ca^{2+}. Distance geometry and simulated annealing methods were used to derive 23 convergent structures from a set of 302 interproton distance restraints and two torsion angle measurements. A high-resolution structure, with the backbone root mean square deviation to the geometric average of the 23 structures of 0.6 ± 0.1 Å, contains a linear α-helix from Gla 3 to Lys 15. Gla residues 3, 7, 10, and 14 are aligned in a linear array on one face of the helix. A genetic algorithm was applied to determine the calcium positions in conantokin G, and the conantokin G/Ca^{2+} complex refined by molecular simulation. Upon binding of Ca^{2+} to γ-carboxyglutamic acid, conantokin G undergoes a conformational transition from a distorted curvilinear 3_{10} helix to a linear α-helix. Occupancy of the metal binding sites, defined by γ-carboxyglutamic acids, results in formation of a calcium−carboxylate network that linearizes the helix and exposes the hydrophobic amino acids on the opposite face of the helix.

γ-Carboxyglutamic acid is a metal-binding amino acid whose synthesis is dependent upon vitamin K. Of the classes of proteins that contain γ-carboxyglutamic acid, the vitamin K-dependent blood coagulation and regulatory proteins have been most thoroughly studied (for review, see ref *1*). In these proteins, 10−12 γ-carboxyglutamic acid residues are located in a domain at the N-terminus of the protein. Upon addition of calcium ions, these proteins undergo a structural transition that is associated with the expression of a phospholipid binding site (*2*−*4*). The Gla domain confers upon these proteins a structure that facilitates calcium-mediated interaction of the protein with membrane surfaces (*5*). The three-dimensional structures of the Gla domain of prothrombin (*6*), factor VII (*7*), and factor IX (*8*, *9*) reveal a common polypeptide fold in which the γ-carboxyglutamic acid side chains are oriented internally to chelate a cluster of calcium ions that are not exposed to solvent. The stabilization of this conformer of the vitamin K-dependent proteins by calcium ions is associated with their interaction with membrane surfaces (*10*), a property critical for the biological activity of these proteins. Glutamic acid or aspartic acid substituted for γ-carboxyglutamic acid at a number of critical residues eliminates the membrane binding properties (*5*, *11*, *12*).

It remains unclear whether the functional role of γ-carboxyglutamic acid in other vitamin K-dependent proteins is as a calcium-binding amino acid. To address this potential role for γ-carboxyglutamic acid, we are studying the role of γ-carboxyglutamic acid found in the conotoxins of the marine snail *Conus*. These marine invertebrates elaborate a complex series of neurotoxins in their venom (*13*). The sequences of five conotoxins—conantokin G, conantokin T, Ctx Tx-VIIA, conotoxin GS, and bromosleeper peptide—have been previously shown to contain γ-carboxyglutamic acid (*14*−*19*). Furthermore, γ-carboxyglutamic acid is in high abundance in crude conotoxins, where it represents about 3% of the amino acid content (J. Stenflo, personal communication). Conantokin G is a 17-residue conotoxin from the venom of *Conus geographus*, a fish-hunting cone snail whose venom has been known to cause human fatalities. Conantokin G contains five γ-carboxyglutamic acid residues; Gla 3 and Gla 4 are critical to neurotoxin function (*20*). We have recently determined a high-resolution three-dimensional structure of conantokin G in the absence of metal ions (*21*). This 17-residue conotoxin, well-structured despite the ab-

[†] This work was supported in part by funds from the Marine Biological Laboratory, by grants from the National Institutes of Health (HL38216, HL42443, HL18834, and HL06350), by a research fellowship from the Heart and Stroke Foundation of Canada to A.C.R., and by a grant for computer time from the North Carolina Supercomputing Center.

[‡] The coordinates reported in this paper have been deposited in the Brookhaven Protein Data Bank under filename 1awy.

[§] Department of Biochemistry, Tufts University School of Medicine.

[||] Department of Medicine, Tufts University School of Medicine, and Center for Hemostasis and Thrombosis Research, New England Medical Center.

[⊥] NIEHS and University of North Carolina.

[▽] Marine Biological Laboratory.

[⊗] Abstract published in *Advance ACS Abstracts,* December 1, 1997.

S0006-2960(97)01855-2 CCC: $14.00

sence of disulfide bonds and calcium ions, is characterized by a partial loop centered on Gla 3 and Gla 4, a distorted type I turn between Gln 6 and Gln 9, and two type I turns involving Gla 10−Arg 13 (*21*). A recent study of the conantokin G/Ca^{2+} structure has proposed the general elements of the secondary structure, suggesting the presence of both 3_{10} and α-helix in a flexible curvilinear helix (*22*). The tertiary structure of the peptide was insufficiently resolved to permit analysis of the role of γ-carboxyglutamic acid. In its physiologic role as a fish neurotoxin, conantokin G is reactive with the *N*-methyl-D-aspartate (NMDA) receptor in the extracellular space in the presence of calcium. Since conantokin G binds calcium ions with a K_d of about 2−3 mM (*23*) and undergoes a conformational transition upon binding to calcium ions (*20*, *22*−*24*), we wished to determine the structure of the conantokin G/Ca^{2+} complex at high resolution in order to compare the apo structure with the metal-bound structure and infer the role of the γ-carboxyglutamic acid residues. In the current study, we demonstrate that the solution structure of the conantokin G/Ca^{2+} complex is dominated by a linear α-helix. Upon calcium binding to the Gla residues and the formation of the carboxylate−Ca^{2+} network, conantokin G undergoes a structural transition from a distorted curvilinear 3_{10} helix to a linear α-helix. The binding of Ca^{2+} to conantokin G leads to the exposure of a hydrophobic region on the opposite face of the helix.

MATERIALS AND METHODS

Peptide Synthesis and Identification. Conantokin G was synthesized and its covalent structure confirmed as previously described (*21*).

NMR Spectroscopy. Three samples of conantokin G in 90% H_2O were used: (1) conantokin G (1.2 mM) dissolved in 10% D_2O, pH 5.60, and 25 mM acetate-d_4; (2) conantokin G (5.8 mM) dissolved in 10% D_2O, pH 5.60, 100 mM NaCl, 25 mM acetate-d_4, and 58 mM $CaCl_2$; and (3) conantokin G (1.89 mM) dissolved in 10% D_2O, pH 5.60, 25 mM acetate-d_4, 150 mM NaCl, and $CaCl_2$ (as indicated); in addition, this sample was heated to 55 °C at pH 7.0 in the presence of Chelex 100 to displace any tightly bound metal ions prior to the addition of $CaCl_2$. Samples 1 and 2 were pretreated with Chelex 100 at 25 °C to remove trace metal ion contaminants. A sample in D_2O was prepared by lyophilizing a solution of conantokin G (10.0 mM) containing 150 mM $CaCl_2$, pH 5.60, and 25 mM acetate-d_4 in 99.8% D_2O and redissolving it in an equal volume of 99.96% D_2O. Spectra were collected at 25 °C on a Bruker AMX-500 spectrometer with a proton frequency of 500.14 MHz. The carrier frequency was set on the water resonance, which was suppressed using presaturation.

The effect of Ca^{2+} on conantokin G was evaluated by one- and two-dimensional NMR spectroscopy as a function of Ca^{2+} concentration. Following the addition of $CaCl_2$ to the sample, the sample was equilibrated for 10 min before data collection. One dimensional data were acquired at 25 °C with 16K real data points, with 256 summed scans, a spectral width of 4629.63 Hz, and processed by applying a squared sine bell window function shifted by 30°. At each $CaCl_2$ concentration, two-dimensional total correlation (TOCSY) (*25*) spectra were recorded employing the MLEV-17 spin lock sequence (*26*) with a mixing time of 35 ms for 32 summed scans. A nuclear Overhauser effect (NOESY) (*27*) spectrum with a mixing time of 400 ms was recorded at a calcium to conantokin G concentration of 3:1, allowing sequence-specific assignment of the individual γ-protons.

Two-dimensional NOESY spectra were recorded with mixing times of 150, 250, and 400 ms at 25 °C. A total of 2048 or 4096 real data points were acquired in *t*2, with 512 time-proportional phase incrementation (TPPI) (or States-TPPI) increments in *t*1, with a spectral width of 8064.52 Hz in both dimensions. A total of 128 summed scans was collected with a relaxation delay of 1.3 s. Spectra were multiplied with a sine bell window function shifted by 30° in *t*2 (applied over 1024 points) and a sine bell window function shifted by 30° in *t*1 (applied over all 512 acquired points) and zero-filled to a 2K by 1K (real) matrix using the Bruker NMR processing program. NOESY cross-peak intensities were converted into three distance classes (1.7−3.0 Å, strong; 1.7−4.0 Å, medium; 3.0−5.0 Å, weak) and calibrated using published methods (*28*). Briefly, the NOE intensities for $d_{\alpha N(i,i+1)}$ and $d_{NH\alpha(i,i)}$ were compared to known distances in a range of secondary structural elements (*28*). The $d_{NN(i,i+1)}$ distances were used to confirm the calibration and were observed to be approximately 2.8 Å for residues in an α helix and about 4 Å otherwise; these results are in agreement with Wüthrich (*29*). The NOE intensities were observed to be proportional to the mixing time employed. Therefore the isolated spin pair approximation was valid for distance determination. Nonstereospecifically assigned atoms were treated as pseudoatoms and given correction distances (*29*). Distance restraint information was extracted from NOESY spectra with different mixing times. Comparison of the short and long mixing-time spectra was used to control for spin diffusion effects. TOCSY spectra were recorded and processed using identical parameters as the NOESY, with the exception that a 35 ms mixing time was used in collecting 128 summed scans. A double quantum filtered correlation (DQF-COSY) (*30*) spectrum was recorded with 4096 real *t*2 points, 40 summed scans, and 768 TPPI increments. The spectrum was multiplied by sine bell window functions shifted by 30° in *t*2 and 30° in *t*1 and zero-filled to a 2K by 1K (real) matrix. In addition, a similar set of experiments (DQF-COSY, TOCSY, and NOESY) was performed on a 10 mM peptide sample in 99.96% D_2O at a noncorrected pH of 5.60.

Sequence-specific resonance assignments were made in two stages. The intraresidue spin systems were identified using the $^1H-^1H$ through-bond connectivities found in TOCSY and DQF-COSY spectra. The sequential assignment of residues was completed on the basis of sequential $d_{\alpha N}$, and d_{NN} NOE connectivities (*29*). The NOESY spectrum collected on a sample in D_2O was used to reveal protons that were near the resonance of H_2O protons. The NOE contacts were classified into "intraresidue" for NOEs within a residue; "sequential and short-range" for contacts between the backbone and side-chain protons of residue *i* with residue $i + 1$; "medium-range" for *i*, $i + 2$ connnectivities; and "long-range" for *i*, $i + 3$ and *i*, $i + 4$ NOEs between protons on residues separated by three or more amino acid positions in the sequence.

Structure determination used a set of 302 distance restraints (271 intraresidue and sequential; 31 short-, medium-, and long-range), and 2 χ_1 angles. A combination of distance geometry and simulated annealing methods (*31*) were used to generate 25 structures, of which 23 converged using the

DGII program of InsightII (Molecular Simulations, San Diego, CA). The simulated annealing protocol was performed with a force constant of 1 kcal mol^{-1} $Å^{-2}$ applied as described elsewhere (*32*). The final total error function value was 0.10 ± 0.0013 kcal mol^{-1}. Nonconverged structures had energies of > 0.175 kcal mol^{-1}. The average structure for the ensemble was calculated using the Analysis program of InsightII. Average root-mean-square deviation (RMSD) values following superimposition of the backbone atoms of each structure with the geometric average reflected the quality of the structures determined. In addition, the coherence of torsion angles among different structures was evaluated. The average torsion angle was measured by a vector addition method (*28*). An order parameter, *S*, equals 1.0 when the torsion angle is the same in all structures, whereas an order parameter near zero indicates disorder at that position.

Refinement of Conantokin G/Ca^{2+} Structure and Placement of Calcium Ions. The genetic algorithm (*9*) was used to identify the calcium positions in the solution structure of conantokin G. The complete set of oxygen−oxygen distances within 6 Å was used to initially place the calcium ions at the midpoints of two oxygen atoms. A total of 161 midpoint positions were found that fit these constraints. Each structure in each generation was energy-minimized using AMBER (*33*). After appropriate convergence of the procedure, the low-energy structure found by the genetic algorithm was used as the starting structure for a molecular dynamics refinement. The molecular dynamics simulations were performed using explicit water (*9*) and the Particle-Mesh Ewald (PME) method incorporated into AMBER to accommodate the long-range electrostatic forces (*34*). During the refinement, the newly placed calcium ions and water molecules were energy-minimized followed by 100 picosecond (ps) molecular dynamics simulations. Next, another 200 ps simulation was carried out on the calcium ions, water, and all side-chain atoms while the backbone of the polypeptide was fixed to the structure defined by NMR. An average structure was generated from the trajectory of the last 100 ps simulations; this structure defined the calcium ion network. Computations were performed on a Silicon Graphics Power Challenge workstation and on a CRAY T90 at the North Carolina Supercomputing Center.

RESULTS

Conantokin G, prepared by solid-phase peptide synthesis and subsequently fully characterized (*21*), corresponds to the entire polypeptide sequence of conantokin G as isolated from the venom of *Conus geographus*: NH_2-Gly-Glu-Gla-Gla-Leu-Gln-Gla-Asn-Gln-Gla-Leu-Ile-Arg-Gla-Lys-Ser-Asn-NH_2. The peptide was rendered metal-free using Chelex 100. The one-dimensional NMR spectra of the metal-free conantokin G and the conantokin G/Ca^{2+} complex at pH 5.6 were collected at 25 °C (Figure 1). In the one dimensional spectrum of the apo conantokin G, the proton resonances are spectrally disperse, with many of the amide and α-proton resonances shifted from their random coil values (*29*). We have previously shown that this conotoxin in the absence of metal ions is highly structured (*21*). Since conantokin G binds Ca^{2+} (*23*), we were interested in determining the spectral perturbations introduced with the addition of Ca^{2+} to conantokin G and the effect of Ca^{2+} on conantokin G structure.

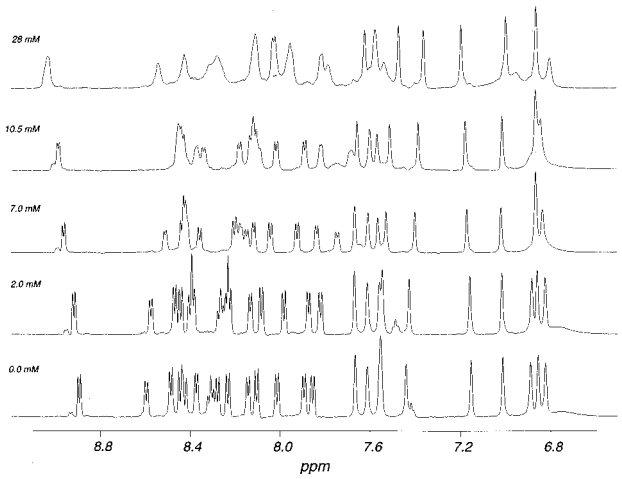

FIGURE 1: One-dimensional ^1H NMR spectra of conantokin G. The sample contained 1.1 mM conantokin G (metal-free), 25 mM acetate-d_4, and 10% D_2O, pH 5.60 in H_2O. The spectra were acquired with 1024 scans at 25 °C. Each 1D spectrum represents the amide region of conantokin G following the addition of specified concentrations of $CaCl_2$ to the sample. All spectra were processed with a sine bell window function shifted by 30°, over 16K real data points, and the solvent peak was removed with a sine bell convolution function. $CaCl_2$ concentrations appear to the left of each spectrum.

Skjaerbaek et al. (*22*) have recently suggested that conantokin G may bind Ca^{2+} with very high affinity and that the variable spectroscopic results obtained on apoconantokin G may relate to varying degrees of success in the removal of bound Ca^{2+} from the peptide. To demonstrate that our apoconantokin G was metal-free after treatment with Chelex 100, we thermally denatured conantokin G by adjusting a peptide solution to 55 °C in the presence of Chelex 100 and subsequently obtained a 1D NMR spectrum of the peptide solution. This spectrum was identical to that previously described for the apoconantokin G (*21*), thus verifying that this peptide was free of metal ions.

Calcium-Induced Structural Transition: Effect of Ca^{2+} on the γ- and α-Protons of γ-Carboxyglutamic Acid Residues. The γ-carboxyglutamic acid residues, distributed along the polypeptide of conantokin G, served as probes of the calcium-induced conformational transition. Since the γ-H and α-H of the five γ-carboxyglutamic acids were spectrally degenerate within complex envelopes in one-dimensional NMR spectra, these resonances were studied in two-dimensional TOCSY experiments in order to obtain definitive assignments and chemical shifts as a function of calcium ion concentration. After resonance assignment without added Ca^{2+}, calcium was added to the conantokin G solution and the α- and γ-protons of γ-carboxyglutamic acid were monitored as a function of Ca^{2+} concentration. Since the exchange of conantokin G and Ca^{2+} at equilibrium is rapid on the NMR time scale, the observed chemical shift of proton resonances represents the average between the chemical shift of a specific proton in the apoconantokin G and the chemical shift of that proton in the conantokin G/Ca^{2+} complex. During this Ca^{2+} titration, changes in the chemical shift of α- and γ-protons associated with the γ-carboxyglutamic acid residues were evident. The α-protons of the five Gla residues had chemical shifts of 4.06−4.16 ppm in the metal-free conantokin G (Figure 2A). The α-protons of Gla 4, Gla 7, and Gla 14 underwent upfield shifts of about 0.14−0.16 ppm upon formation of the conantokin G/Ca^{2+} complex. The

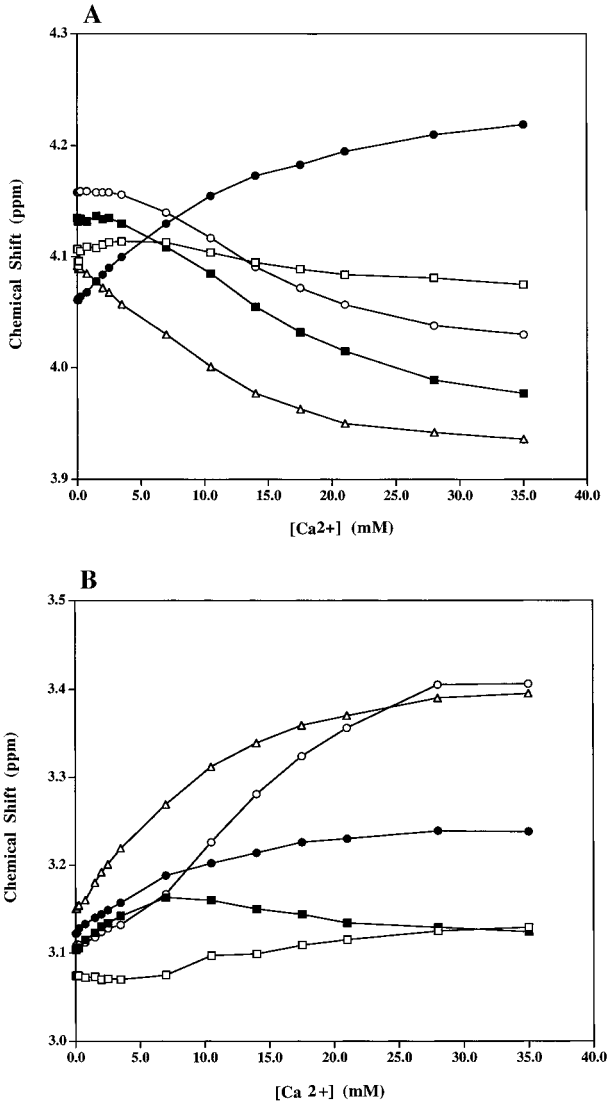

FIGURE 2: Change in chemical shifts of Gla residues as a function of calcium concentration. (A) Chemical shift of the α-H of each Gla residue in conantokin G as a function of Ca^{2+} concentration; (B) chemical shift of the γ-H of each Gla residue in conantokin G as a function of Ca^{2+} concentration. Gla 3, □; Gla 4, ■; Gla 7, ○; Gla 10, ●; Gla 14, △.

chemical shift of the α-proton of Gla 3 was not significantly altered, while the chemical shift of the α-proton of Gla 10 was shifted downfield about 0.14 ppm. Fitting of these data to a two-state model (*35*) is consistent with an equilibrium constant, *K*, of 2 mM describing the Ca^{2+}-induced conformational equilibrium. The change in chemical shift reflects alterations in the secondary structure of the polypeptide backbone upon Ca^{2+} binding.

The chemical shifts of the γ-protons of the five Gla residues, monitored as a function of the Ca^{2+} concentration (Figure 2B), also served as reporters for the Ca^{2+}-induced conformational transition. The chemical shift changes (0.11−0.25 ppm) of the γ-protons of Gla 10 and Gla 14 were characterized by a binding isotherm that fit a simple two-state model. This two-state model had an equilibrium constant, *K*, of 2 mM. Ca^{2+} induces an upfield chemical shift of 0.32 ppm of the γ-proton of Gla 7 but the binding isotherm cannot be fitted to a simple two-state model. In contrast, there were small changes in the chemical shifts of the γ-protons of Gla 3 and Gla 4. Ca^{2+} binding to free γ-carboxyglutamic acid was associated with a small upfield chemical shift of the γ-protons (data not shown). Therefore, the chemical shifts of the γ-proton of the five γ-carboxyglutamic acid residues in conantokin G are primarily due to perturbations of these protons by alterations in the structure of the γ-carboxyglutamic acid side chain, while the perturbations of the α-protons of these γ-carboxyglutamic acid residues is primarily due to the formation of secondary structure in the polypeptide backbone. These results suggest that the three-dimensional structure of the N-terminal region of conantokin G, including Gla 3 and Gla 4, is modestly altered by Ca^{2+}. However, Gla 7, Gla 10, and Gla 14 participate in a large conformational transition.

Three-Dimensional Structure of the Conantokin G/Ca^{2+} Complex. To define both the secondary structure and the tertiary structure of conantokin G, with special emphasis on the γ-carboxyglutamic acid side chains and their role in calcium binding, we solved the solution structure of conantokin G in the presence of saturating concentrations of calcium ions by two-dimensional homonuclear ^{1}H NMR spectroscopy. Standard NOESY, TOCSY, and DQF-COSY experiments were used to assign the resonances (*26*, *29*) (Figure 3). For the majority of residues, TOCSY spectra showed backbone amide to α and β connectivities, the only exceptions being those α protons buried underneath the water resonance, and the intraresidue connectivities to glycine 1, glutamine 6, and glutamine 9. In some cases, the NH−γH connectivities were also observed. The proton resonance assignments are presented in Table S-1 in the supporting information. From the set of backbone assignments, all remaining nonintraresidue, nonsequential NOE cross-peaks could be identified.

The spectral resolution limited determination of $^3J_{HN\alpha}$ to greater than 7.5 Hz and precluded measurement for Asp 8, Gln 9, and Gla 10 with extremely broad line widths. The major secondary structure in this peptide was assessed as α-helical by analysis of sequential $\alpha H-NH_{(i,i+1)}$, $NH-NH_{(i,i+1)}$, $\beta H-NH_{(i,i+1)}$, and $\alpha\beta_{(i,i+3)}$ connectivities (Figure 4).

Structure calculations by distance geometry and simulated annealing methods employed 302 distance restraints, of which 271 were derived from intraresidue and sequential backbone NOEs and 31 derived from medium- and long-range NOEs. Strong interactions and NOEs between the α proton of residue *i* and the β proton and amide of residue *i*, $i + 3$ and *i*, $i + 4$ identify regions of helicity between Gla 3 and lysine 15. Throughout the helical region of the molecule, numerous NOE cross-peaks between side-chain protons of Gla 3, Gla 4, Gla 7, and Gla 10 define well-ordered structures of these side chains (Figure 4). These NOE cross-peaks between neighboring hydrophilic side chains are indicative of a localized charged region on one face of the molecule. In addition, two χ1 angle restraints were used. Of the resulting 25 structures, 23 possessed an average distance violation of 0.015 Å with no NOE violations greater than 0.2 Å. These 23 structures are overlaid in Figure 5. The RMSD to the average is 0.6 ± 0.1 Å for the well-defined backbone residues of 23 final structures. The correlation and mean ϕ and ψ angles for each residue were measured for the family of structures. The majority of backbone torsion angles had correlations near 100% for residues 3−15. Otherwise, there is fraying of the N-termini and C-termini on either end of the α-helix.

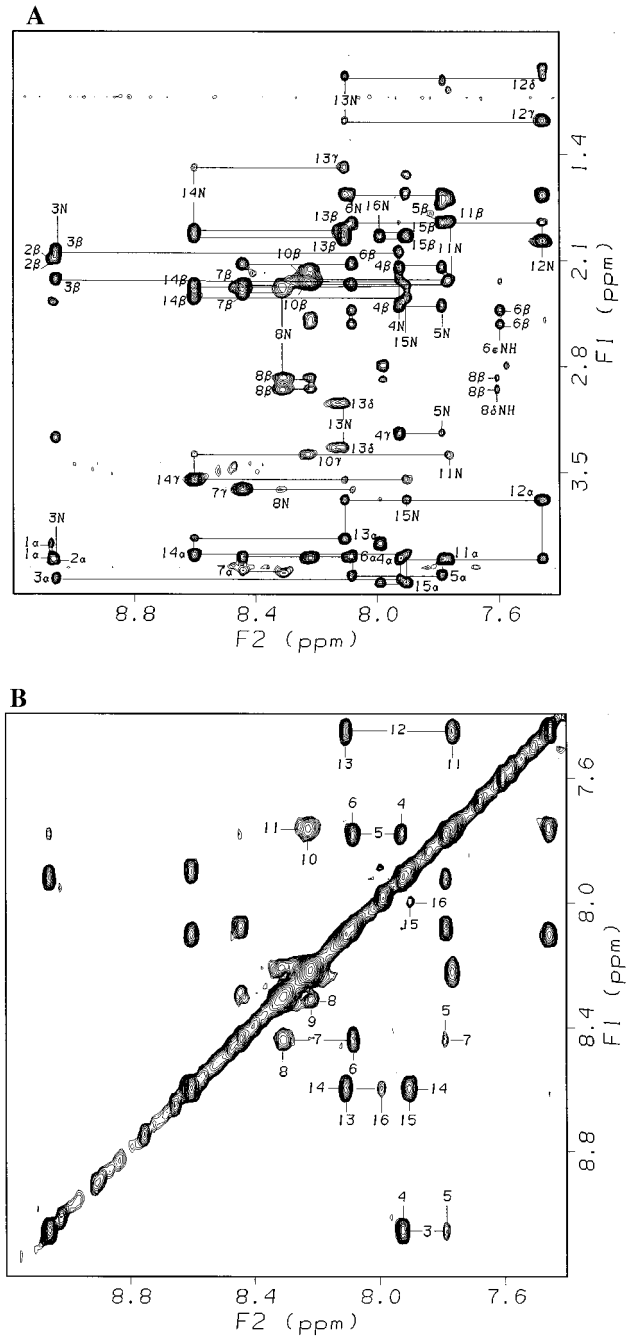

FIGURE 3: NOESY spectra. (A) Region of the two-dimensional NOESY spectrum (400 ms mixing time) of the conantokin G/Ca^{2+} complex. Connectivities are illustrated between intraresidue and sequential α-$NH_{(i,i+1)}$, with the intraresidue NH-α connectivities labeled with the amino acid number. In addition, interresidue and short-range connectivities are identified. (B) Amide−amide region of the NOESY spectrum of the conantokin G/Ca^{2+} complex. All connectivities involving sequential (i, $i + 1$) and (i, $i + 2$) amide protons are labeled with the residue number. The amide−amide connectivities commence at Gla 3 and extend through to Ser 16 with the cross-peak between Gln 9 and Gla 10 obscured by the diagonal.

A ribbon diagram of the conantokin G/Ca^{2+} complex demonstrates the linear α-helix that characterizes the secondary structure (Figure 6). A space-filling model of this conantokin G structure emphasizes that the γ-carboxglutamic acid residues (red) are distributed along one side of the α-helix to form a linear arrangement of eight carboxylate moieties (Figure 7). Gla 4 is adjacent to this linear array.

Refinement of Conantokin G Structure and Placement of Calcium Ions. Conantokin G is a Ca^{2+}-binding polypeptide,

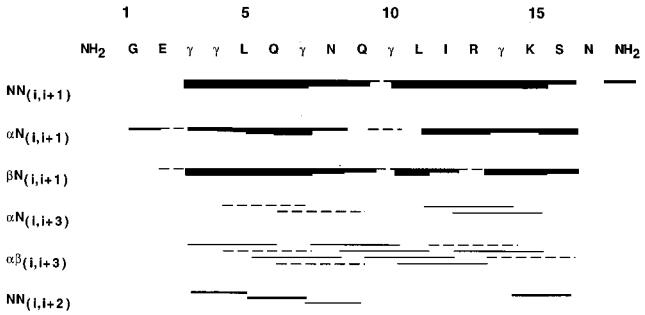

FIGURE 4: Summary of sequential and short- to medium-range connectivities generated from NOE peaks. The thickness of the bars represents the intensity of the sequential and NN(i, $i + 1$), αN(i, $i + 1$), and βN(i, $i + 1$) NOE connectivities. Spectral degeneracy that precludes unique identification of a connectivity is identified by a dashed line. Through-space connectivities typical of α-helices [αN(i, $i + 3$), $\alpha\beta$(i, $i + 3$), and NN(i, $i + 2$)] are diagrammed.

where the number of Ca^{2+} bound is 2−3 (*23*). The binding isotherms were complex and could not be defined uniquely. To place the positions of these Ca^{2+}, the previously described genetic algorithm (*9*) was applied and possible structures were refined by molecular dynamics simulation with the Particle-Mesh Ewald method to accommodate long-range electrostatic forces (*34*). With the conantokin G structure of Figure 7 as the starting structure, the average structures of conantokin G bound to 3, 4, or 5 Ca^{2+} were obtained. The best model was obtained with 4 Ca^{2+}/peptide, and this structure at equilibrium during the simulation is presented in Figure 8. In this simulation, the four Ca^{2+} ions charge-neutralized the conantokin G/Ca^{2+} structure. The salient feature of this conantokin G/Ca^{2+} complex is the intricate oxygen−calcium ion network. Four calcium ions, labeled A−D, are liganded through carboxylate oxygens. Calcium ion A is coordinated by two carboxylate oxygens of Gla 3 and one carboxylate oxygen of Gla 4; calcium ion B is coordinated by one carboxylate oxygen of Gla 3 and two carboxylate oxygens of Gla 7; calcium ion C is coordinated by two carboxylate oxygens of Gla 7 and two carboxylate oxygens of Gla 10; calcium ion D is coordinated by one carboxylate oxygen of Gla 10 and two carboxylate oxygens of Gla 14. In this model, each Ca^{2+} is liganded by three or four carboxylate oxygens contributed by two γ-carboxyglutamic acid residues. The organization of this calcium−carboxylate network is shown in Figure 9. Significant noncovalent structure is imposed on conantokin G through this carboxylate−Ca^{2+} network. γ-Carboxyglutamic acid is uniquely suited to participate in the formation of this network.

DISCUSSION

There have been several studies of conantokin G focused on the influence of calcium ions on the secondary structure of the polypeptide and the metal-binding properties of this conotoxin (*20*, *22*−*24*). To date, the role of γ-carboxyglutamic acid in calcium binding and the mechanism by which γ-carboxyglutamic acid binding to calcium ions might mediate the structural changes in conantokin G that are important for receptor recognition have not been elucidated. To assess the role of γ-carboxyglutamic acid in calcium binding, we determined a high-resolution structure of conantokin G in the presence of calcium ions and compared it to the high-resolution structure that we determined in the absence of metal ions (*21*). Furthermore, we examined the role of γ-carboxyglutamic acid in defining the Ca^{2+} binding

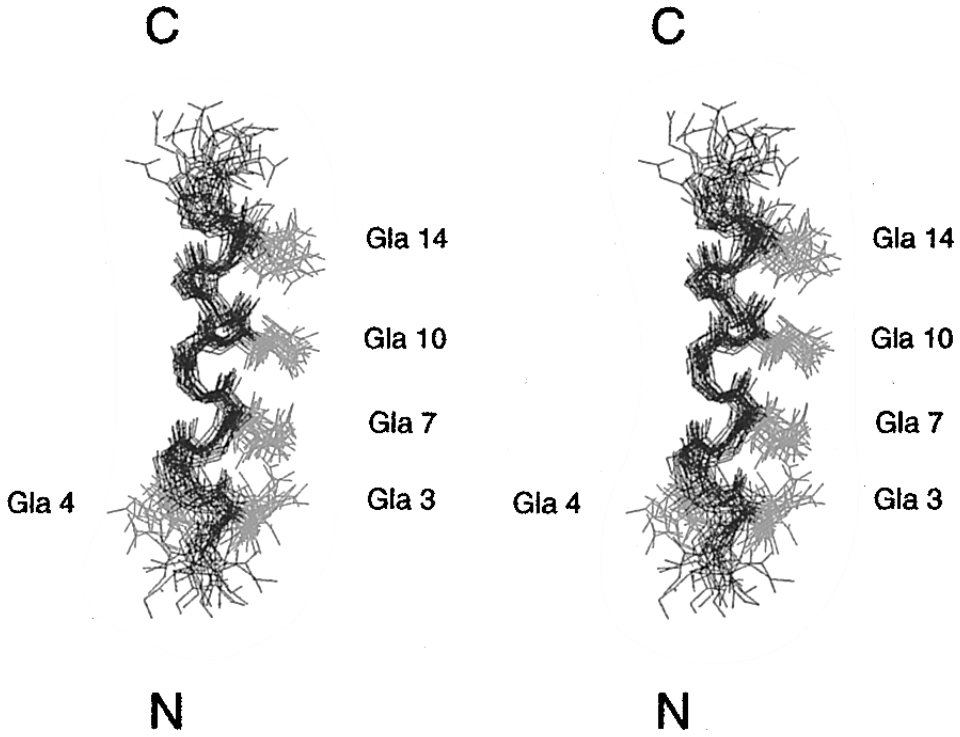

FIGURE 5: Stereoview overlay of the 23 calculated structures for conantokin G/Ca^{2+} complex. All backbone structures and the γ-carboxyglutamic acid side chains are shown superimposed with the geometric average structure. The polypeptide backbone is illustrated in black and the γ-carboxyglutamic acid side chains are in red. The polypeptide backbone root-mean-square deviation compared to the average is 0.6 ± 0.1 Å. Each Gla residue and the N- and C-termini are labeled.

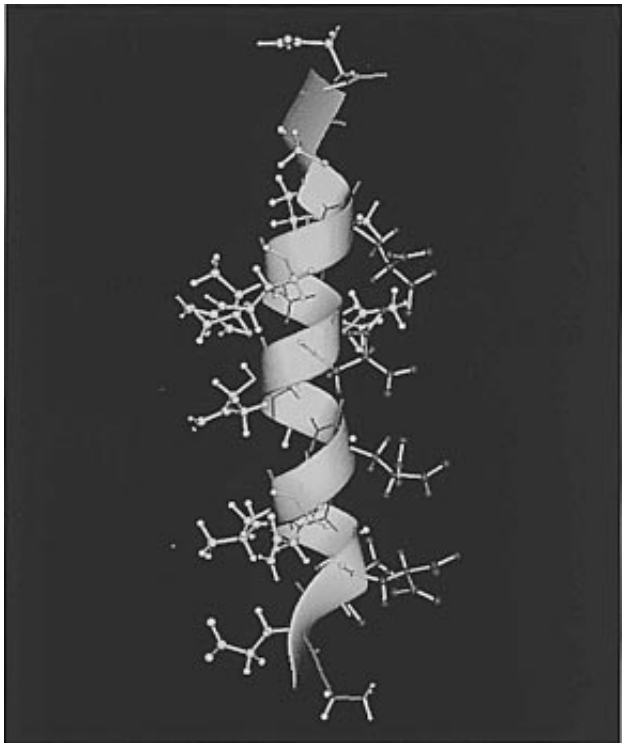

FIGURE 6: Backbone structure of conantokin G. The backbone of the lowest-energy structure of the conantokin G/Ca^{2+} is represented as a ribbon. The polypeptide is oriented with the N-terminus pointing down. A linear α-helix extends from Gla 3 to Lys 15. All residues are white except γ-carboxyglutamic acids (red).

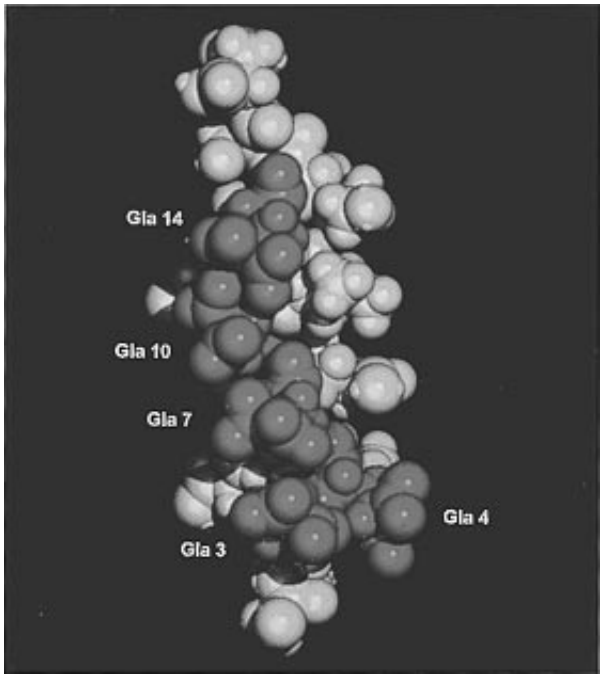

FIGURE 7: Space-filling model of the Ca^{2+}-stabilized conformer of conantokin G. The Gla residues (red) define the Gla patch. The five Gla residues are labeled by residue number. Gla 3, 7, 10, and 14 form a linear array; Gla 4 is adjacent to and contiguous with the patch.

sites, to better understand why glutamic acid residues do not preserve conantokin G function when substituted for γ-carboxyglutamic acid residues (*20*).

In this study, we define a high-resolution tertiary structure of the conantokin G/Ca^{2+} complex that is sufficiently well-resolved to analyze the role of the γ-carboxyglutamic acid side chains. This three-dimensional structure, with a RMSD of 0.6 Å, is characterized by a linear α-helix from residue 3 to 15, with a straight axis in all of the calculated structures. Furthermore, we demonstrate that four γ-carboxyglutamic acid residues—Gla 3, Gla 7, Gla 10, and Gla 14—are aligned on one face of the α-helix to form a continuous surface and that Gla 4 is adjacent to this Gla patch. The lower-resolution

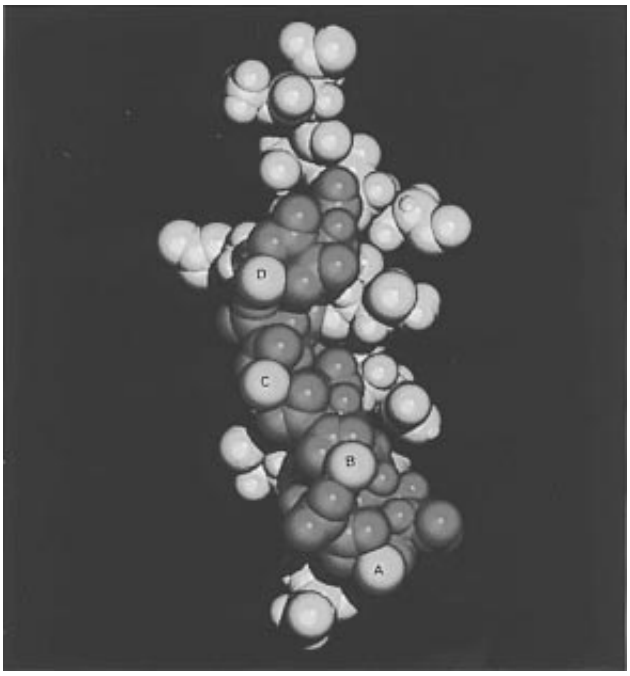

FIGURE 8: Model of the Ca^{2+}/conantokin G structure, with the addition of bound calcium ions. Calcium placement was determined using a genetic algorithm as described in Materials and Methods. The Gla residues in the Gla patch are shown in red and the bound calciums (A−D) are shown in yellow. The lowest energy structure is illustrated as a space-filling model.

NMR experiment of Skjaerbaek et al. (*22*) is limited to an analysis of the secondary structure. Their structure of the conantokin G/Ca^{2+} complex, with a RMSD of 1.68 Å defined by 161 distance restraints, has both 3_{10} helix and α-helix components. They suggest that there are two well-defined helices toward the N- and C-termini that are connected by a somewhat flexible midregion. Skjaerbaek et al. (*22*) suggest that their NMR data may not be sufficient to define the relative orientations of sections of the helix or that a helix extending nearly the length of the polypeptide has genuine flexibility. On the basis of our high-resolution structure, we believe that the former interpretation is correct: there are insufficient data to define the tertiary structure of the polypeptide and the smaller number of observed constraints may be responsible for the curvature in the backbone of their conantokin G structure.

The Gla domain of the vitamin K-dependent blood coagulation proteins is a specialized module that is responsible for the calcium-dependent interaction of these proteins with membrane surfaces. In the absence of metal ions, these proteins fail to bind to membrane surfaces. Upon addition of metal ions, they undergo two conformational transitions that can be monitored by fluorescence quenching or circular dichroism or with conformation-specific antibodies (*2*−*4*, *36*). The first conformational transition occurs upon occupancy of metal binding sites by most divalent metal ions (*36*). The second conformational transition requires calcium ions and is associated with the expression of the membrane binding site. The Gla domain of the metal-free form of factor IX shows stable structure between residues 6 and 9, the disulfide-linked loop from Cys 18 to Cys 23, and a helix from residue 35 to 46 (*32*). The γ-carboxyglutamic acid residues are exposed to solvent. However, in the calcium-stabilized complex of factor IX, factor VII, and prothrombin (*6*−*9*), the Gla side chains are reoriented inward, as ligands

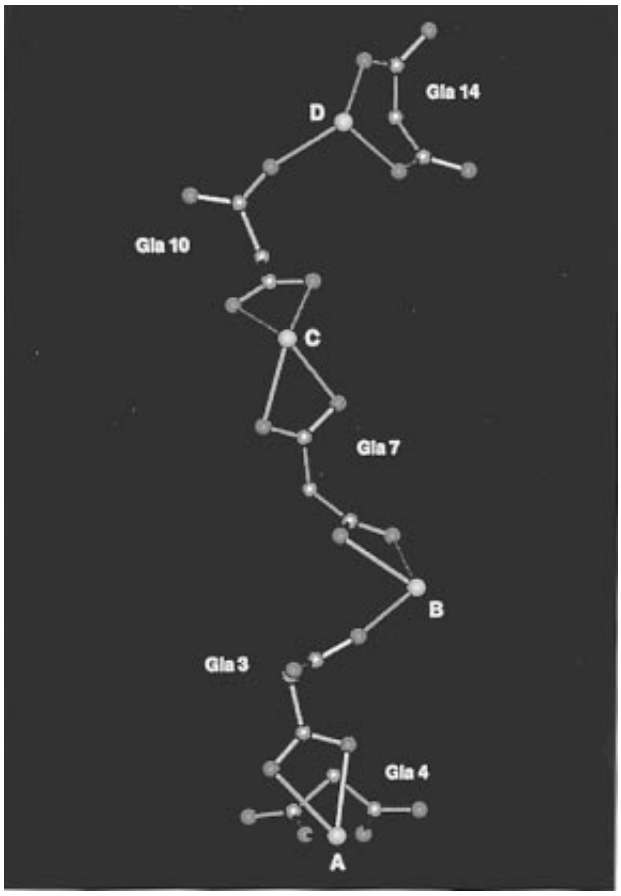

FIGURE 9: Calcium ion−carboxylate coordination network. Each calcium ion is liganded by three or four carboxylate oxygens. The bidentate structure of γ-carboxyglutamic acid enables the formation of a complex network involving multiple γ-carboxyglutamic acid residues and multiple calcium ions.

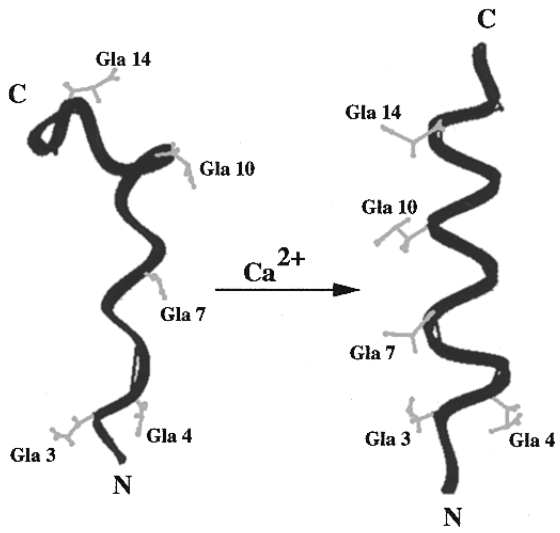

FIGURE 10: Calcium-induced structural transition in conantokin G. The formation of a network of carboxylate ligands bound to Ca^{2+} is associated with the stabilization of a unique conformer and the exposure of solvent-accessible hydrophobic amino acids that are available for membrane interaction.

for internal calcium ions, some of which are not solvent-exposed. This has similarly been proposed for factor X (*37*). Thus, γ-carboxyglutamic acid residues play a key role in the vitamin K-dependent blood coagulation proteins as ligands for calcium and stabilization of a calcium-bound conformer in which the N-terminal loop containing the membrane binding site is exposed (*10*).

In contrast, the conantokin G/Ca^{2+} complex shows a distinct and unique organization of Gla residues. The Gla side chains are completely exposed to solvent, and Gla 3, Gla 7, Gla 10, and Gla 14 are nearly perfectly aligned in a linear array. Only Gla 4 is separate from this array. Although γ-carboxyglutamic acid remains a chelator of calcium ions and this interaction stabilizes a unique conformer of the polypeptide, the structural motif is clearly distinct from that of the vitamin K-dependent blood coagulation proteins. The energy associated with the formation of the Gla carboxylate−Ca^{2+} network effects a transition from the distorted 3_{10} helix structure and from the hydrophobic collapse that is responsible for the curvilinear axis of the apoconantokin G structure (Figure 10). In the formation of the network of Ca^{2+} liganded by carboxylate groups of Gla residues, the helix is straightened, the hydrophobic interactions on the opposite side of the helix are perturbed, and this hydrophobic patch is more exposed to solvent. By comparison of the structures of the apoconantokin G and the conantokin G/Ca^{2+} complex, the environment around the side chains of Gla 3 and Gla 4 is only modestly altered during this Ca^{2+}-induced conformational transition. Indeed, we demonstrate minimal alterations in the chemical shifts of the γ-protons of these γ-carboxyglutamic acids during the conformational transition. However, the polypeptide backbone from Gla 3 to Lys 15 undergoes a substantial structural transition to realize the α-helix, and the chemical shifts of the γ-protons of Gla 7, Gla 10, and Gla 14 and the α-protons of Gla 4, Gla 7, Gla 10, and Gla 14 are influenced by this transition.

It is likely that the Ca^{2+}-liganded form of the conotoxin is biologically active. Thus, a common feature of the vitamin K-dependent blood coagulation proteins and conantokin G is the formation of a network of carboxylate ligands bound to Ca^{2+}. This network, first described in vitamin K-dependent proteins by Tulinsky and colleagues (*6*), is associated with the stabilization of a unique conformer and the exposure of solvent-accessible hydrophobic amino acids that are available for membrane interaction. γ-Carboxyglutamate−Ca^{2+} interaction in conantokin G has a critical role in defining the physiologically relevant structure as well.

ACKNOWLEDGMENT

We thank Drs. Johan Stenflo and Eva Czerwiec for many helpful discussions and Margaret Jacobs for the peptide synthesis.

SUPPORTING INFORMATION AVAILABLE

Table S-1, containing the proton resonance assignments for the metal-free conantokin G peptide (1 page). Ordering information is given on any current masthead page.

REFERENCES

1. Furie, B., and Furie, B. C. (1988) *Cell 53,* 505−518.
2. Nelsestuen, G. L., Broderius, M., and Martin, G. (1976) *J. Biol. Chem. 251,* 6886−6893.
3. Bloom, J. W., and Mann, K. G. (1978) *Biochemistry 17,* 4430−4438.
4. Furie, B., Provost, K., Blanchard, R. A., and Furie, B. C. (1978) *J. Biol. Chem. 253,* 8980−8987.
5. Esmon, C. T., Suttie. J. W., and Jackson, C. M. (1975) *J. Biol. Chem. 250,* 4095.
6. Soriano-Garcia, M., Padmanabhan, K., de Vos, A. M., and Tulinsky, A. (1992) *Biochemistry 31,* 2554−2566.
7. Banner, D. W., D'Arcy, A., Chene, C., Winkler, F. K., Guha, A., Konigsberg, W. H., Nemerson, Y., and Kirchofer, D. (1996) *Nature 380,* 41−46.
8. Freedman, S. J., Furie, B. C., Furie, B., and Baleja, J. D. (1995) *Biochemistry 34,* 12126−12137.
9. Li, L., Darden, T. A., Freedman, S. J., Furie, B. C., Furie, B., Baleja, J. D., Smith, H., Hiskey, R. G., and Pedersen, L. G. (1997) *Biochemistry 36,* 2132−2138.
10. Freedman, S. J., Blostein, M. D., Baleja, J. D., Jacobs, M., Furie, B. C., and Furie, B. (1996) *J. Biol. Chem. 271,* 16227−16236.
11. Zhang, L., and Castellino, F. J. (1993) *J. Biol. Chem. 268,* 12040−12045.
12. Ratcliffe, J., Furie, B., and Furie, B. C. (1993) *J. Biol. Chem. 268,* 24339−24345.
13. Olivera, B. M., Rivier, J., Clark, C., Ramilo, C., Corpuz, G., Bogadie, F., Woodward, S., Hillyard, D., and Cruz, L. (1990) *Science 249,* 257−263.
14. McIntosh, J. M., Olivera, B. M., Cruz, L. J., and Gray, W. R. (1984) *J. Biol. Chem. 259,* 14343−14346.
15. Yanagawa, Y., Abe, T., Satake, M., Odani, S., Suzuki, J., and Ishikawa, K. (1988) *Biochemistry 27,* 6256−6262.
16. Haack, J. A., Rivier, J., Parks, T. N., Mena, E. E., Cruz, L. J., and Olivera, B. M. (1990) *J. Biol. Chem. 265,* 6025−6029.
17. Fainzilber, M., Gordon, D., Hasson, A., Spira, M. E., and Zlotkin, E. (1991) *Eur. J. Biochem. 202,* 589.
18. Nakamura, T., Yu, Z., Fainzilber, M., and Burlingame, A. L. (1996) *Protein Sci. 5,* 524−530.
19. Craig, A. G., Jimenez, E. C., Dykert, J., Nielsen, D. B., Gulyas, J., Abogadie, F. C., Porter, J., Rivier, J. E., Cruz, L. J., Olivera, B. M., and McIntosh, J. M. (1997) *J. Biol. Chem. 272,* 4689−4698.
20. Zhou, L.-M., Szendrei, G. I., Fossom, L. H., Maccacchini, M.-L., Skolnick, P., and Otvos, L. (1996) *J. Neurochem. 66,* 620−628.
21. Rigby, A. C., Baleja, J. D., Furie, B. C., and Furie, B. (1997) *Biochemistry 36,* 6906−6914.
22. Skjaerbaek, N., Nielsen, K. J., Lewis, R. J., Alewood, P., and Craik, D. J. (1997) *J. Biol. Chem. 272,* 2291−2299.
23. Prorok, M., Warder, S. E., Blandl, T., and Castellino, F. J. (1996) *Biochemistry 35,* 16528−16534.
24. Myers, R. A., McIntosh, J. M., Imperial, J., Williams, R. V., Oas, T., Haack, J. A., Hernandez, J.-F., Rivier, J., Cruz, L., and Olivera, B. M. (1990) *J. Toxicol. Toxin Rev. 9,* 179−202.
25. Braunschweiler, L., and Ernst, R. R. (1983) *J. Magn. Reson. 53,* 521−528.
26. Bax, A., and Davis, D. G. (1985) *J. Magn. Reson. 65,* 355−359.
27. Jeener, J., Meier, B. H., Bachman, P., and Ernst, R. R. (1979) *J. Chem. Phys. 71,* 4546−4553.
28. Hyberts, S. G., Goldberg, M. S., Havel, T. F., and Wagner, G. (1992) *Protein Sci. 1,* 736−751
29. Wüthrich, K. (1986) *NMR of Proteins and Nucleic Acids,* Wiley-Interscience, New York.
30. Rance, M., Sorensen, O. W., Bodenhausen, G., Wagner, G., Ernst, R. R., and Wüthrich, K. (1983) *Biochem. Biophys. Res. Commun. 117,* 479−485.
31. Havel, T. F. (1991) *Prog. Biophys. Mol. Biol. 56,* 43−78.
32. Freedman, S. J., Furie, B. C., Furie, B., and Baleja, J. D. (1995) *J. Biol. Chem. 270,* 7980−7987.
33. Pearlman, D. A., Case, D. A., Caldwell, J. W., Ross, W. S., Cheatham, T. E., III, Ferguson, D. M., Seibel, G. L, Singh, U. C., Weiner, P. K., and Kollman, P. A. (1995) AMBER4.1, University of California, San Francisco, CA.
34. Essemann, U., Perera, L., Berkowitz, M. L., Darden, T., Lee, H., and Pedersen, L. G. (1995) *J. Chem. Phys. 103,* 8577−8593.
35. Gilbert, G. E., Furie, B. C., and Furie, B. (1990) *J. Biol. Chem. 265,* 815−822.
36. Borowski, M., Furie, B. C., Bauminger, S., and Furie, B. (1986) *J. Biol. Chem. 261,* 14969−14975.
37. Sunnerhagen, M., Forsén, S., Hoffrén, A.-M., Drakenberg, T., Teleman, O., and Stenflo, J. (1995) *Nat. Struct. Biol. 2,* 504−509.

BI9718550